

Elastic and total reaction cross sections of oxygen isotopes in Glauber theory

B. Abu-Ibrahim,^{1,2} S. Iwasaki*,³ W. Horiuchi,³ A. Kohama,¹ and Y. Suzuki⁴

¹RIKEN Nishina Center, RIKEN, Wako-shi, Saitama 351-0198, Japan

²Department of Physics, Cairo University, Giza 12613, Egypt

³Graduate School of Science and Technology, Niigata University, Niigata 950-2181, Japan

⁴Department of Physics, Graduate School of Science and Technology, Niigata University, Niigata 950-2181, Japan

We systematically calculate the total reaction cross sections of oxygen isotopes, $^{15-24}\text{O}$, on a ^{12}C target at high energies using the Glauber theory. The oxygen isotopes are described with Slater determinants generated from a phenomenological mean-field potential. The agreement between theory and experiment is generally good, but a sharp increase of the reaction cross sections from ^{21}O to ^{23}O remains unresolved. To examine the sensitivity of the diffraction pattern of elastic scattering to the nuclear surface, we study the differential elastic-scattering cross sections of proton- $^{20,21,23}\text{O}$ at the incident energy of 300 MeV by calculating the full Glauber amplitude.

PACS numbers: 25.40Cm, 21.10.Gv, 25.60.Dz, 25.60.-t, 24.10.Ht

Keywords:

I. INTRODUCTION

Studies on neutron-rich unstable nuclei have been attracting much attention both experimentally and theoretically. These studies are motivated, for example, by that we want to understand the nuclear structure and excitation mode of the neutron-rich nuclei as well as a role played by them in forming heavy elements in stars. Binding energy, radius and density distribution, among others, are basic quantities to determine the nuclear property. Reactions of unstable neutron-rich nuclei with a proton target are, therefore, of current interest as they are at present a major means to probe the matter densities of exotic nuclei, particularly the region of the nuclear surface. If one appropriately selects the incident energies, protons could be more sensitive to the neutron distributions than to the proton distributions of nuclei.

The Glauber theory [1] offers a powerful and handy framework for the description of high energy nuclear reactions. This theory describes proton-nucleus reactions very well. Usually a calculation based on the Glauber theory is performed using a one-body density calculated from a nuclear wave function. However, Bassel *et al.* [2] calculated Glauber's scattering amplitude using a Slater determinant wave function, and were able to examine the effect of Pauli blocking, which is impossible to discuss using just the one-body density.

Recently, we have analyzed the total reaction cross sections of carbon isotopes on both ^{12}C [3] and proton [4] targets using the Glauber theory. The densities of the carbon isotopes are constructed from Slater determinants generated from a phenomenological mean-field potential or two types of dynamical models, core+ n and core+ $n+n$ models, which go beyond the mean-field model.

Data on the cross sections of the oxygen isotopes up

to the dripline nucleus ^{24}O are available at high energies [5, 6]: The cross sections show a gentle increase with increasing neutron number from ^{16}O to ^{21}O and then an abrupt increase up to ^{23}O . On the other hand, several theoretical studies on the matter radii predict a mild increase of the radii with increasing neutron number. The calculations have been performed for the isotopes up to $N = 12$ [7], and much further [8, 9, 10, 11]. As the spin-parity systematics of the ground states of the oxygen isotopes indicates that the $d_{5/2}$ single-particle orbit seems fairly stable, we first analyze the cross section data using a model similar to that of the previous study, that is, assuming the mean-field potentials that reproduce the nucleon separation energies. The interest of this analysis is to examine the extent to which the theory can explain the characteristic behavior of the cross sections.

One of the advantages of the Glauber theory is that the same input as used in the reaction cross section calculation is readily applicable for the calculation of the differential cross section of elastic-scattering. The diffraction pattern in the differential cross section is expected to depend on the diffuseness of the nuclear surface. Therefore we also study elastic scattering of the oxygen isotopes on a proton target. The case of p - ^{16}O scattering serves as a testing ground of our model. We then predict the differential cross sections of p - $^{20,21,23}\text{O}$ elastic scattering. The differential elastic-scattering cross section data of p - ^{20}O is available only at low energy, such as ~ 30 MeV per nucleon [12].

This paper is organized as follows. The reaction models for the calculation of the total reaction and elastic-scattering cross sections are recapitulated in Sect. II. The construction of the densities of the oxygen isotopes is explained in Sect. III. We present the calculation of the total reaction cross sections of the oxygen isotopes in Sect. IV. The differential cross sections for neutron-rich oxygen isotopes are given in Sect. V. A summary is given in Sect. VI. Appendix A presents the densities of the oxygen isotopes which are obtained using the Slater determinants constructed from the harmonic-oscillator single-

*Present address: Intertrade Co., Ltd., Chuo-ku, Tokyo 104-0032, Japan

particle orbits. Appendix B explains the calculation of the p -nucleus elastic-scattering amplitude using a Slater determinant.

II. PHASE SHIFT FUNCTIONS IN THE GLAUBER MODEL

The Glauber theory provides us with an excellent framework to describe high energy reactions [1]. The p -nucleus elastic-scattering amplitude is given by

$$F(\mathbf{q}) = \frac{iK}{2\pi} \int d\mathbf{b} e^{i\mathbf{q}\cdot\mathbf{b}} \left(1 - e^{i\chi_N(\mathbf{b})}\right), \quad (1)$$

where \mathbf{b} is the impact parameter vector perpendicular to the beam (z) direction, \mathbf{K} the initial momentum of the relative motion, and \mathbf{q} the momentum transferred from the projectile to the target. Here we neglect the p -nucleus Coulomb potential, because its effect appears only in the extreme forward direction for a light target. The nuclear part of the optical phase-shift function is given by

$$e^{i\chi_N(\mathbf{b})} = \langle \Psi_0 | \prod_{i=1}^A \left[1 - \frac{1 + \tau_{3i}}{2} \Gamma_{pn}(\mathbf{b} - \mathbf{s}_i) - \frac{1 - \tau_{3i}}{2} \Gamma_{pp}(\mathbf{b} - \mathbf{s}_i) \right] | \Psi_0 \rangle, \quad (2)$$

where Ψ_0 is the intrinsic (translation-invariant) A -nucleon wave function of the nuclear ground state, and \mathbf{s}_i is the projection onto the xy -plane of the nucleon coordinate relative to the center-of-mass of the nucleus. Here τ_{3i} is 1 for neutron and -1 for proton.

The profile function, Γ_{pN} , for the pp and pn elastic scatterings, is usually parameterized in the form

$$\Gamma_{pN}(\mathbf{b}) = \frac{1 - i\alpha_{pN}}{4\pi\beta_{pN}} \sigma_{pN}^{\text{tot}} \exp\left(-\frac{\mathbf{b}^2}{2\beta_{pN}}\right), \quad (3)$$

where α_{pN} is the ratio of the real to the imaginary part of the pN scattering amplitude in the forward direction, σ_{pN}^{tot} is the pN total cross sections, and β_{pN} is the slope parameter of the pN differential cross section. These parameters for different incident energies are tabulated in Refs. [3, 4].

The differential cross section of the p -nucleus elastic-scattering is given by

$$\frac{d\sigma}{d\Omega} = |F(\mathbf{q})|^2, \quad (4)$$

and the total reaction cross section of the p -nucleus collision is calculated from

$$\sigma_R = \int d\mathbf{b} \left(1 - |e^{i\chi_N(\mathbf{b})}|^2\right). \quad (5)$$

In the optical limit approximation (OLA), the p -nucleus scattering phase-shift function is simply given

using the proton density $\rho_p(\mathbf{r})$ and the neutron density $\rho_n(\mathbf{r})$ as follows

$$e^{i\chi^{\text{OLA}}(\mathbf{b})} = \exp[i\chi_p(\mathbf{b}) + i\chi_n(\mathbf{b})], \quad (6)$$

where χ_p (χ_n) denotes the phase shift due to the protons (neutrons) inside the nucleus

$$\begin{aligned} i\chi_p(\mathbf{b}) &= - \int d\mathbf{r} \rho_p(\mathbf{r}) \Gamma_{pp}(\mathbf{b} - \mathbf{s}), \\ i\chi_n(\mathbf{b}) &= - \int d\mathbf{r} \rho_n(\mathbf{r}) \Gamma_{pn}(\mathbf{b} - \mathbf{s}). \end{aligned} \quad (7)$$

We will evaluate Eq. (2) completely for a Ψ_0 that is given by a Slater determinant comprising harmonic-oscillator single-particle orbits, and use it in Sect. V.

III. DENSITIES OF OXYGEN ISOTOPES

Compared to the carbon isotopes, where the competition of the $1s_{1/2}$ and $0d_{5/2}$ orbits appears to play an important role to determine their structure, the spin-parity systematics of the oxygen isotopes indicates that the $0d_{5/2}$ orbit is lower than the $1s_{1/2}$ orbit in the ground states up to ^{22}O . The configurations for the oxygen isotopes are thus assumed to be given according to the shell-model as follows: The nucleus ^{16}O is a doubly magic nucleus occupying the $0s_{1/2}$, $0p_{3/2}$ and $0p_{1/2}$ orbits, and ^{15}O has a neutron hole in the $0p_{1/2}$ orbit. The nucleus ^AO with $16 < A \leq 22$ has $A - 16$ valence neutrons in the $0d_{5/2}$ orbit, and for $A=23, 24$ it has six neutrons in the $0d_{5/2}$ orbit as well as $A - 22$ neutrons in the $1s_{1/2}$ orbit. We assume the spin-parity of the ground state of ^{21}O is $\frac{5}{2}^+$ though it is not yet confirmed experimentally.

The single-particle orbits are generated from the mean-field potential containing central and spin-orbit potentials. The Coulomb potential is added for protons. The strength of the spin-orbit potential is set to follow the standard value, whereas the strength of the central part is chosen so as to reproduce the separation energy of the last nucleon. See Ref. [3] for details. This prescription is called an “ S_n model” hereafter. This model apparently ignores the pairing effect, which gives larger separation energy for the even- N nucleus than for the odd- N nucleus. Therefore the S_n model tends to predict a too large size for the odd- N isotope. To remedy this problem, we also test another one, called an “ $\langle S_n \rangle$ model”, which fits the average separation energy for the nucleons in the last orbit. For example, in the case of ^{19}O in which three neutrons occupy the $0d_{5/2}$ orbit, the average neutron separation energy to be fitted is one third of a sum of the neutron separation energies of $^{17,18,19}\text{O}$, and likewise the average proton separation energy to be fitted is one half of a sum of the proton separation energies of ^{19}O and ^{18}N . The center-of-mass motion is taken into account in order to obtain the intrinsic density. See Ref. [3] for detail.

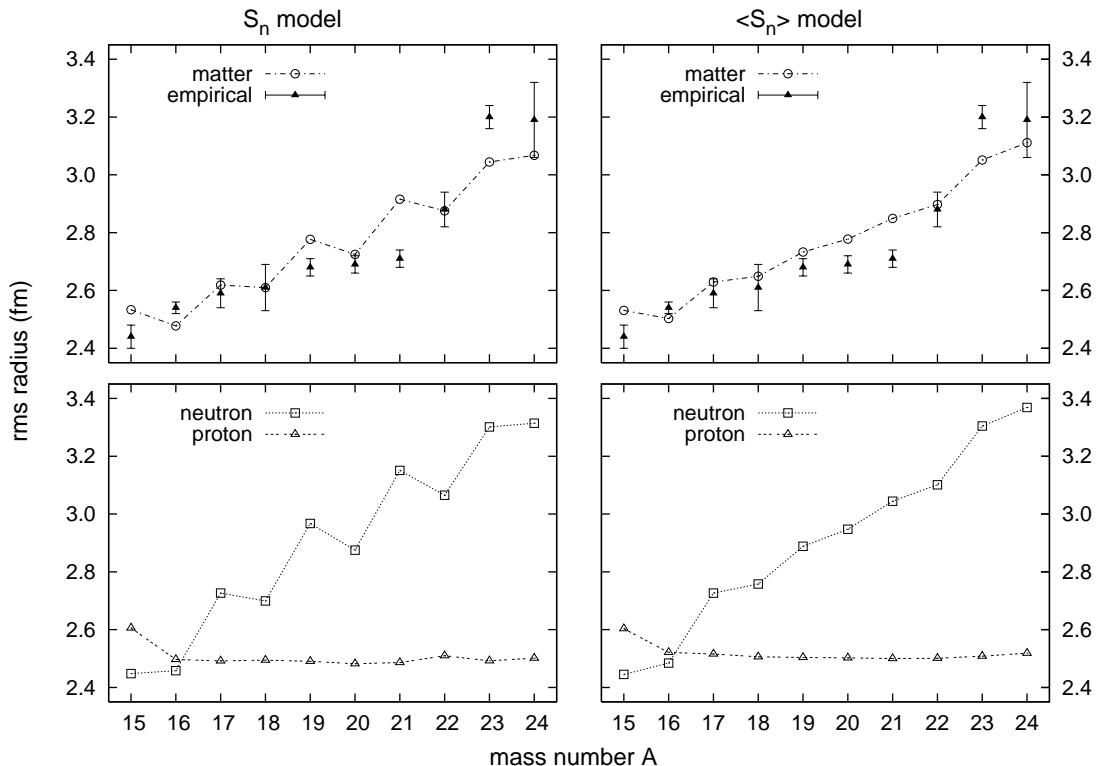


FIG. 1: The matter, neutron and proton root-mean-square radii of the oxygen isotopes calculated with the S_n and $\langle S_n \rangle$ models. The empirical values are taken from Ref. [5].

We also use harmonic-oscillator single-particle orbits in Sect. V to examine the differential cross section.

Figure 1 compares the matter, neutron and proton root-mean-square (rms) radii of the oxygen isotopes (r_m , r_n , and r_p , respectively) calculated in the S_n and $\langle S_n \rangle$ models. Clearly the strong even-odd staggering seen in the neutron radius of the S_n model becomes mild in the $\langle S_n \rangle$ model, and the matter radii in the latter model seem to be in better agreement with those extracted from a model-dependent analysis of the interaction cross section data [5]. Noticeable discrepancies appear at ^{21}O and ^{23}O . The theory predicts a smaller radius for ^{21}O but a larger radius for ^{23}O than the empirical values. We will see in Sect. IV that this discrepancy directly appears in the comparison of the reaction cross sections. The charge radii of $^{16,17,18}\text{O}$ calculated in the $\langle S_n \rangle$ model using the finite size correction of the nucleon are found to be 2.64, 2.63, 2.62 fm, which are slightly smaller than the measured values, 2.718(21), 2.662(26), 2.727(20) fm [13], respectively.

IV. RESULTS FOR TOTAL REACTION CROSS SECTIONS

Before showing results of calculation for the total reaction cross sections of the oxygen isotopes, we first com-

pare in Fig. 2 the theoretical p - ^{16}O total reaction cross section to experiment. The OLA approximation is used. The cross sections calculated at higher energies are in reasonable agreement with the data. A slight underestimation is consistent with the fact that the density of ^{16}O gives a slightly smaller radius compared to the experimental value. The theory predicts about 15% larger cross sections at lower energies, which is very similar to the one found in the analysis of the p - ^{12}C total reaction cross section [4]. The reason for this discrepancy is due

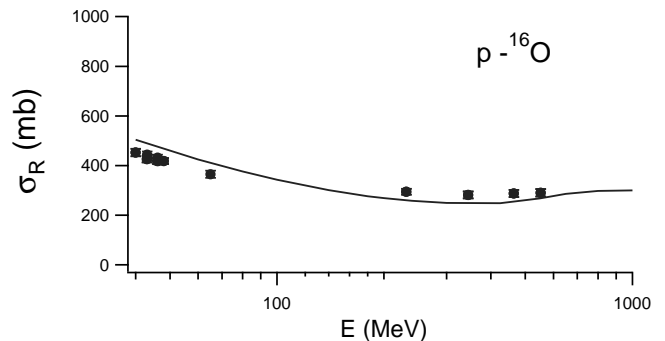


FIG. 2: Comparison of the p - ^{16}O total reaction cross sections calculated in the OLA with experiment. The data are taken from Ref. [14, 15].

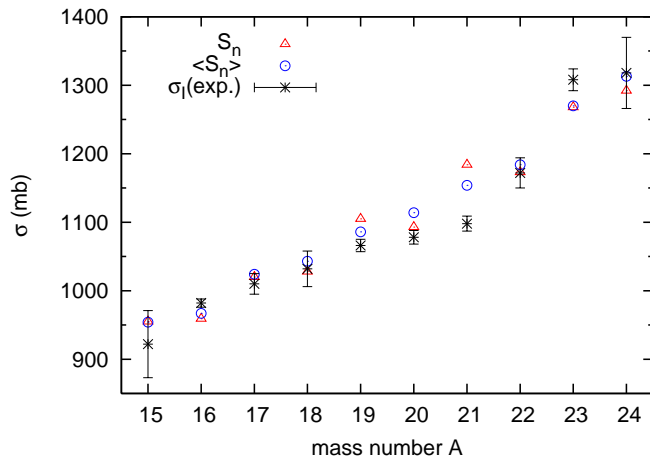


FIG. 3: (Color online) Total reaction cross sections for the oxygen isotopes incident on a ^{12}C target. The incident energy is about 1 GeV per nucleon except for ^{15}O . The calculation is based on the NTG approximation. The experimental data are taken from Ref. [5].

to the limitation of applying the Glauber theory to the reaction at the energy lower than 100 MeV [16].

Figure 3 displays the total reaction cross sections of the oxygen isotopes incident on a ^{12}C target. The calculated values are based on the NTG approximation [3], which includes higher-order corrections missing in the OLA calculation, and they are compared to the interaction cross sections measured at incident energies around 1 GeV per nucleon [5]. The energy per nucleon is, however, about 710 MeV in the case of ^{15}O . The density used for ^{12}C is the same as in Ref. [3]. The $\langle S_n \rangle$ model seems to give slightly better results than the S_n model.

For a comparison between theory and experiment, it is important to realize that it is the total reaction cross section that is calculated and not the interaction cross section. The interaction cross section does not include the contribution from the inelastic excitation of a projectile nucleus to a particle-bound state, whereas the total reaction cross section includes this contribution. It is in general not trivial to estimate the difference between the two cross sections [17], but they are not expected to be very different at high energies [18, 19]. As already noted in the comparison of the matter radii, the theory can reproduce the increase of the cross sections up to ^{20}O but fails to reproduce the sharp rise of the cross section from ^{21}O to ^{23}O . It was noted in Ref. [20] that the latter discrepancy cannot be explained in any theoretical models. See Fig. 4 of Ref. [20] as well as the calculation of Ref. [21].

The sharp rise in the interaction cross section at ^{23}O has led to some controversial issues for the understanding of its origin. It was conjectured in Refs. [20, 22] that a core nucleus ^{22}O could be substantially modified in ^{23}O if described with a $^{22}\text{O}+n$ model and also that the spin-parity of the ground state of ^{23}O might be $\frac{5}{2}^+$ rather than

$\frac{1}{2}^+$. Motivated by this, several experiments have been performed, which all support $\frac{1}{2}^+$ [23, 24, 25, 26, 27], as adopted in the present study. Namely, the configuration of the ground state of ^{23}O is dominated by a $1s_{1/2}$ neutron coupled to $^{22}\text{O}(0^+)$ and an excited configuration of $(1s_{1/2})^2(0d_{5/2})^{-1}$ appears as a resonance lying very close to the $n+^{22}\text{O}$ threshold [25, 27]. The enhancement of the cross section from ^{21}O to ^{23}O thus remains an open question to be explained.

As another possibility for getting information on nuclear size, particularly near its surface, we will examine in the next section the p -nucleus elastic scattering.

V. ELASTIC-SCATTERING CROSS SECTIONS

In the previous section we calculated the total reaction cross section for the oxygen isotopes using the phenomenological mean-field potential. Though the $\langle S_n \rangle$ model was found to give nuclear sizes that reproduce the cross sections reasonably well, the increase of the cross section from ^{21}O to ^{23}O was not explained. The p - ^{20}O elastic scattering has recently been measured at the National Institute of Radiological Sciences (NIRS) in Japan [28]. In this section we study the differential cross section of the p -oxygen isotope elastic-scattering in order to examine how sensitive the differential cross section is to the nuclear size.

To this end, it is more convenient if we can adjust the nuclear size more flexibly. Thus we use harmonic-oscillator single-particle wave functions instead of the orbits determined from the separation energies as was done in Sect. III. The size parameters ν_p and ν_n of the harmonic-oscillator wave functions are first determined so as to reproduce the proton and neutron rms radii of the $\langle S_n \rangle$ model and then, by changing the ν_n value to fit the total reaction cross section, we examine the extent to which the differential cross section is altered. Table I lists the radii and the total reaction cross sections of the oxygen isotopes for several sets of ν_p and ν_n values adopted in this section. The r_m , r_n , and r_p values in each row containing a parenthesis correspond to the values of the $\langle S_n \rangle$ model. The density formula obtained from the harmonic-oscillator functions are summarized in Appendix A.

The calculation of the Glauber amplitude (1) for the p -nucleus elastic scattering is explained in Appendix B.

A. Test of the Glauber amplitude: ^{16}O

We present numerical results of the differential cross section for the p - ^{16}O elastic-scattering, and compare it to experiment to study how precisely we can discuss the nuclear size within the Glauber theory.

We start with the calculation of the differential cross section for p - ^{16}O at an incident energy of 1.0 GeV, where

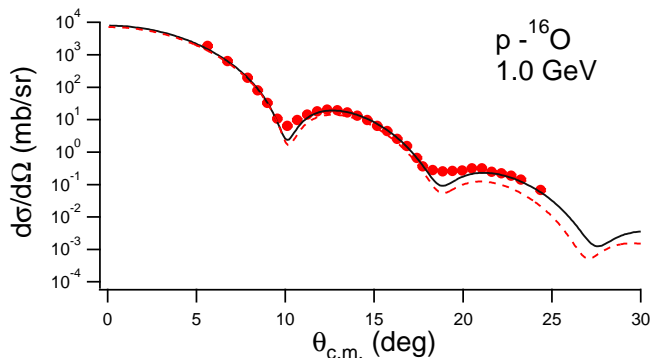


FIG. 4: (Color online) Comparison of the numerical results with the differential elastic-scattering cross section data for p - ^{16}O at $E_p=1.0$ GeV. The solid curve represents the full calculation with the harmonic-oscillator shell-model wave function. The dashed curve represents the calculation with OLA. The data are taken from Ref. [5].

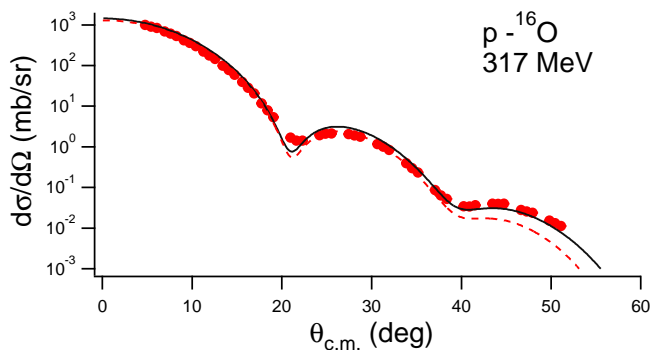


FIG. 5: (Color online) Comparison of the numerical results with the differential elastic-scattering cross section data for p - ^{16}O at $E_p=317$ MeV. See the caption of Fig. 4.

the parameters of the nucleon-nucleon scattering amplitude are well determined. The numerical results of the differential cross sections are shown in Fig. 4. The solid curve represents the result of the full calculation with the harmonic-oscillator shell-model wave function, while the dashed curve shows the cross section calculated in the OLA. Both results agree satisfactorily with the data. The two calculations give no large difference up to the second minimum. This analysis confirms that the p - ^{16}O elastic-scattering cross section is reproduced using the wave function which has a correct size together with the profile function used in the present study.

As the experimental study of p -nucleus elastic scattering at around 300 MeV is considered an interesting and promising project at RIKEN, it is useful to assess the suitability of the profile function at this energy as well. For this purpose we calculate the differential cross section of the p - ^{16}O elastic scattering in this energy region. Figure 5 displays the results of the differential cross section. Both the exact and OLA curves reproduce the data fairly well, similarly to the case of 1 GeV. From these compar-

isons at 300 MeV and 1 GeV, we can conclude that the p -nucleus elastic scattering can reliably be described in the OLA at least up to the second minimum using the present parameters of the profile function.

B. The cross sections of $^{21,23}\text{O}$

As was shown in the previous section, the total reaction cross sections of the oxygen isotopes with a ^{12}C target are reproduced reasonably well, except for the cases of $^{21,23}\text{O}$. In particular, the total reaction cross section of $^{23}\text{O}+^{12}\text{C}$ is calculated to be about 2% smaller than the measured interaction cross section. This may suggest that the $\langle S_n \rangle$ model slightly underestimates the matter radius of ^{23}O . As mentioned at the beginning of the present section, we increase the radius to reproduce the interaction cross section. Three sets of ν_p and ν_n values are listed in Table I. In the case of ^{21}O , the total reaction cross section calculated with the NTG approximation is about 5% larger than the interaction cross section. As ^{21}O has four particle-bound excited states, the difference between the two cross sections could be reduced to some extent. Table I lists a set which fits the interaction cross section of $^{21}\text{O}+^{12}\text{C}$.

Now we examine whether or not the p -nucleus elastic scattering can give us useful information on the matter radius of the nucleus. Figure 6 displays the differential cross section of p - ^{23}O elastic-scattering at $E_p=300$ MeV for the three different matter radii listed in Table I. We focus on the angle of the first peak and the magnitude of the cross section at this angle. As the matter radius increases, the first peak moves to a smaller angle. The angle in degrees (the magnitude of the cross section in mb/sr) of the first peak for the solid, dashed, and dotted curves are 21.5 (4.7), 21.1 (4.2), and 20.5 degree (3.3

TABLE I: The rms radii, in fm, of the matter, neutron and proton density distributions for several oxygen isotopes. The ν_p and ν_n values given in fm are the size parameters of the harmonic-oscillator functions for proton and neutron. See Appendix A. The seventh and eighth columns denote the total reaction cross sections, in units of mb, calculated in the OLA for proton and ^{12}C targets at the incident energy of 1.0 GeV per nucleon. The interaction cross sections taken from Ref. [5] are given in parentheses.

	ν_p	ν_n	r_m	r_n	r_p	$\sigma_R(\text{with } p)$	$\sigma_R(\text{with } ^{12}\text{C})$
^{16}O	1.71	1.71	2.51	2.51	2.51	305	1003 (982±6)
^{20}O	1.70	1.83	2.78	2.94	2.51	369	1135 (1078±10)
^{21}O	1.70	1.87	2.85	3.04	2.51	386	1173 (1098±11)
	1.70	1.67	2.64	2.72	2.51	357	1098
^{23}O	1.70	1.98	3.05	3.30	2.51	429	1267 (1308±16)
	1.70	2.05	3.13	3.41	2.51	440	1302
	1.70	2.15	3.25	3.58	2.51	457	1353

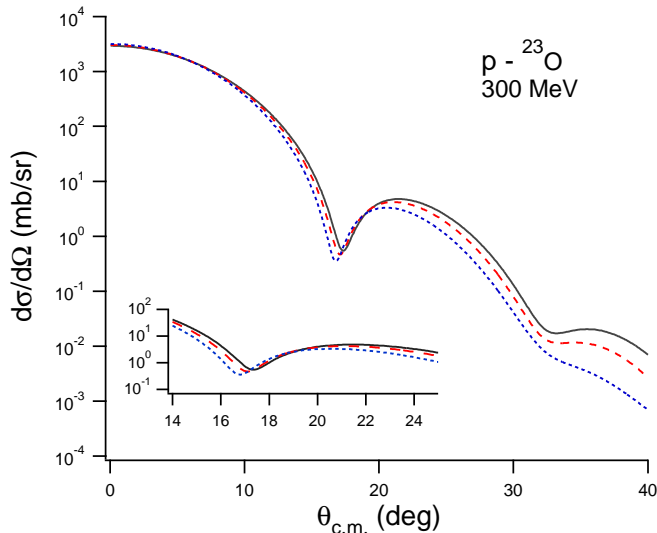


FIG. 6: (Color online) Comparison of the differential elastic-scattering cross sections of p - ^{23}O at $E_p=300$ MeV for different values of nuclear matter radii. The solid curve represents the case with a radius of 3.05 fm, the dashed curve with a radius of 3.15 fm, and the dotted curve with a radius of 3.25 fm. The calculations are carried out with the OLA.

mb/sr), respectively.

The difference, at each first peak angle, between the magnitudes of the cross sections denoted by the solid and dotted curves is about 30%. This value is not small, but, unfortunately the presently estimated experimental uncertainty at this angle for the p - ^{20}O elastic scattering is comparable to this value [28]. The angle shift of the first peak position between the two curves is about 1.0 degree, which might be too small to distinguish experimentally.

We have carried out a similar analysis for the case of ^{21}O . The result is displayed in Fig. 7. The angle (the magnitude of the cross section) of the first peak for the solid and dashed curves are 23.5 (7.3), 22.3 degree (6.4 mb/sr), respectively. Again a high precision experiment will be needed to distinguish which of the above two is favorable.

C. Prediction of the cross section of ^{20}O

Recently the differential cross section of ^{20}O elastic scattering on a proton has been measured at the energy of 300 MeV per nucleon at NIRS [28]. Motivated by this experiment, we predict the elastic and total reaction cross sections of p - ^{20}O .

The Glauber amplitude is calculated fully using the Slater determinant consisting of the harmonic-oscillator single-particle orbits. The size parameter of the harmonic oscillator wave function is chosen to reproduce the radius of ^{20}O given in the $\langle S_n \rangle$ model, as listed in Table I. The result is shown in Fig. 8. The first peak appears at 24.8° and the cross section at the peak is 2.43 mb/sr. As shown

in Fig. 3, the reaction cross section calculated in the NTG approximation is about 30 mb larger than the interaction cross section. It is not clear, however, whether this difference between the two cross sections indicates that the radius used for ^{20}O is slightly too large or not, because a considerable contribution to the reaction cross section is expected from the 12 particle-bound excited states of ^{20}O . In any case the predicted differential cross section near the peak appears consistent with the preliminary data [28].

VI. SUMMARY

We have systematically calculated the total reaction cross sections of the oxygen isotopes, $^{15-24}\text{O}$, on a ^{12}C target at high energies using the Glauber theory. The oxygen isotopes are described with the Slater determinants generated from a phenomenological mean-field potential, which is an extension of our previous work for describing the carbon isotopes [3, 4]. We have introduced two schemes, the S_n model and the $\langle S_n \rangle$ model. The agreement between theory and experiment is generally good, especially in the $\langle S_n \rangle$ model, but the sharp increase of the reaction cross sections from ^{21}O to ^{23}O remains an open question.

As a possible cross section which may depend on the nuclear radius more sensitively than the reaction cross section, we have examined the differential cross sections of the p - $^{20,21,23}\text{O}$ elastic-scatterings at the incident energy of $E_p = 300$ MeV using the full and OLA Glauber amplitudes. The differential cross sections calculated from the two amplitudes are not very different up to the

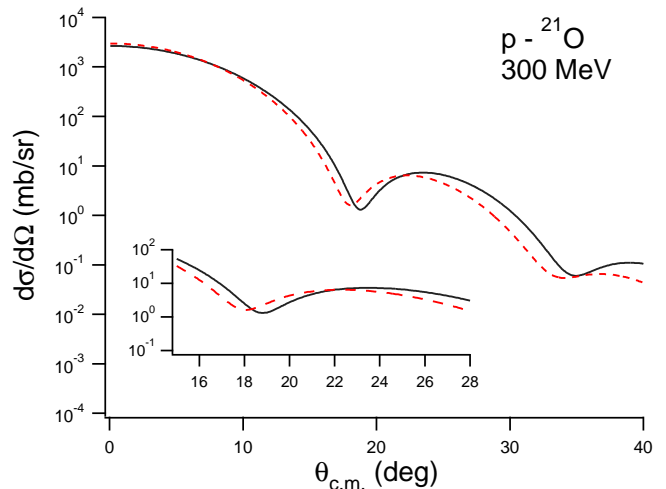


FIG. 7: (Color online) Comparison of the differential elastic-scattering cross sections of p - ^{21}O at $E_p=300$ MeV for different values of nuclear matter radii. The solid curve represents the case with a radius of 2.64 fm, while the dashed curve with a radius of 2.85 fm. The calculations are carried out with the OLA.

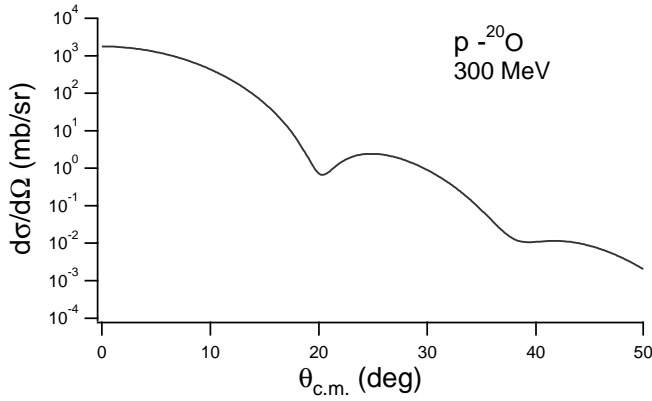


FIG. 8: Prediction of the differential elastic-scattering cross section for p - ^{20}O at $E_p=300$ MeV. The curve represents the full calculation with the harmonic-oscillator shell-model wave function.

second minimum of the angular distribution. We have calculated the total reaction cross sections by varying the nuclear radii so as to be consistent with the observed interaction cross sections, and then analyzed the sensitivity of the differential cross sections to the radii. We find a considerable change in the cross section, but whether it can really be observed or not strongly depends on the precision of the experimental data.

We have predicted the differential cross section for p - ^{20}O elastic-scattering, which has recently been measured. Our prediction appears consistent with the preliminary data. This implies that it is possible to calculate to a good approximation the total reaction and elastic scattering cross sections at high energies.

We are grateful to B. V. Carlson for his careful reading of the manuscript. We acknowledge T. Motobayashi for his encouragement during the course of this work. B. A-I. was supported in part by Japan International Cultural Exchange Foundation (JICEF). W. H. is supported by the Japan Society for the Promotion of Science for Young Scientists. This work was in part supported by a Grant for Promotion of Niigata University Research Projects (2005–2007), and a Grant-in Aid for Scientific Research for Young Scientists (No. 19-3978). One of the authors (Y. S.) thanks the JSPS core-to-core program, Exotic Femto Systems.

APPENDIX A: HARMONIC-OSCILLATOR DENSITY

We briefly explain the method of calculating the neutron or proton intrinsic density which is employed in our paper [3]. We assume a Slater determinant constructed from harmonic-oscillator wave functions. Denoting the Slater determinant by Ψ , we first calculate the neutron or proton density which contains the effect of the center-

of-mass motion

$$\tilde{\rho}(\mathbf{r}) = \langle \Psi | \sum_{i=1}^A \delta(\mathbf{r}_i - \mathbf{r}) P_i | \Psi \rangle, \quad (\text{A1})$$

where \mathbf{r}_i is the nucleon single-particle coordinate and P_i is a projector to either neutron or proton. The single-particle wave function is given by the harmonic-oscillator function

$$\psi_{nljm} = R_{nlj}(r) [Y_l(\hat{\mathbf{r}}) \chi_{1/2}]_{jm}, \quad (\text{A2})$$

where $\chi_{1/2}$ denotes the spin function. If the orbit specified by nlj is not completely filled, we take an average over the z component m , obtaining a spherical density. After some angular momentum algebra we have

$$\tilde{\rho}(\mathbf{r}) = \frac{1}{4\pi} \sum_{nlj} N_{nlj} R_{nlj}^2(r), \quad (\text{A3})$$

where N_{nlj} is the occupation number of the nlj orbit.

To obtain the intrinsic density which has no contribution from the center-of-mass motion, we make use of the fact that the center-of-mass motion $\Psi_{\text{cm}}(\mathbf{X})$ contained in Ψ is factored out as

$$\Psi = \Psi_0 \Psi_{\text{cm}}(\mathbf{X}), \quad (\text{A4})$$

where \mathbf{X} is the center-of-mass coordinate and

$$\Psi_{\text{cm}}(\mathbf{X}) = \left(\frac{A}{\pi\nu^2} \right)^{3/4} \exp\left(-\frac{A}{2\nu^2} \mathbf{X}^2\right). \quad (\text{A5})$$

Then the intrinsic density $\rho(\mathbf{r})$ defined by

$$\rho(\mathbf{r}) = \langle \Psi_0 | \sum_{i=1}^A \delta(\mathbf{r}_i - \mathbf{X} - \mathbf{r}) P_i | \Psi_0 \rangle \quad (\text{A6})$$

is obtained from the following relation [3]

$$\int d\mathbf{r} e^{i\mathbf{k}\cdot\mathbf{r}} \rho(\mathbf{r}) = [\langle \Psi_{\text{cm}} | e^{i\mathbf{k}\cdot\mathbf{X}} | \Psi_{\text{cm}} \rangle]^{-1} \int d\mathbf{r} e^{i\mathbf{k}\cdot\mathbf{r}} \tilde{\rho}(\mathbf{r}). \quad (\text{A7})$$

The radial functions which we need for the oxygen isotopes are

$$\begin{aligned} R_{00}(r) &= \left(\frac{4}{\sqrt{\pi}\nu^3} \right)^{1/2} \exp\left(-\frac{r^2}{2\nu^2}\right), \\ R_{01}(r) &= \left(\frac{8}{3\sqrt{\pi}\nu^5} \right)^{1/2} r \exp\left(-\frac{r^2}{2\nu^2}\right), \\ R_{02}(r) &= \left(\frac{16}{15\sqrt{\pi}\nu^7} \right)^{1/2} r^2 \exp\left(-\frac{r^2}{2\nu^2}\right), \\ R_{10}(r) &= \left(\frac{8}{3\sqrt{\pi}\nu^3} \right)^{1/2} \left(\frac{r^2}{\nu^2} - \frac{3}{2} \right) \exp\left(-\frac{r^2}{2\nu^2}\right). \end{aligned} \quad (\text{A8})$$

We give the examples of $^{21,23}\text{O}$ below. The neutron or proton density of ^{21}O is

$$\begin{aligned} \tilde{\rho}(\mathbf{r}) &= \frac{1}{4\pi} \left[2R_{00}^2 + 6R_{01}^2 + (M-8)R_{02}^2 \right] \\ &= \frac{2}{\pi\sqrt{\pi}\nu^3} \exp\left(-\frac{r^2}{\nu^2}\right) \left[1 + 2\frac{r^2}{\nu^2} + \frac{2(M-8)}{15} \frac{r^4}{\nu^4} \right], \end{aligned} \quad (\text{A9})$$

were M is the number of protons $Z=8$ or the number of neutrons $N=13$. The neutron density for ^{23}O is

$$\begin{aligned}\tilde{\rho}(\mathbf{r}) &= \frac{1}{4\pi} \left[2R_{00}^2 + 6R_{01}^2 + 6R_{02}^2 + R_{10}^2 \right] \\ &= \frac{2}{\pi\sqrt{\pi\nu^3}} \exp\left(-\frac{r^2}{\nu^2}\right) \left[\frac{7}{4} + \frac{r^2}{\nu^2} + \frac{17}{15} \frac{r^4}{\nu^4} \right].\end{aligned}\quad (\text{A10})$$

The corresponding intrinsic density is obtained from the relation (A7). The results are

$$\begin{aligned}\rho(\mathbf{r}) &= 2\left(\frac{u}{\pi\nu^2}\right)^{3/2} \exp\left(-\frac{ur^2}{\nu^2}\right) \\ &\times \left[1 + 3(1-u) + \frac{15}{2}\alpha(1-u)^2 \right. \\ &\left. + 2u^2(1+5\alpha(1-u))\frac{r^2}{\nu^2} + 2\alpha u^4\frac{r^4}{\nu^4} \right],\end{aligned}\quad (\text{A11})$$

for ^{21}O and

$$\begin{aligned}\rho(\mathbf{r}) &= 2\left(\frac{u}{\pi\nu^2}\right)^{3/2} \exp\left(-\frac{ur^2}{\nu^2}\right) \left[\frac{15}{2} - 10u + \frac{17u^2}{4} \right. \\ &\left. + \left(\frac{20u^2}{3} - \frac{17u^3}{3}\right)\frac{r^2}{\nu^2} + \frac{17u^4}{15}\frac{r^4}{\nu^4} \right],\end{aligned}\quad (\text{A12})$$

for ^{23}O . Here $u = A/(A-1)$ and $\alpha = (M-8)/15$.

As is evident, the above derivation assumes that the harmonic-oscillator constant ν is the same for protons and neutrons. When we use different values for these, as in Table I, the intrinsic densities of Eqs. (A11) and (A12) will no longer be exact. However, we have still used these equations to calculate the intrinsic densities in that case.

APPENDIX B: ELASTIC SCATTERING AMPLITUDE

In this appendix, following the method of Refs. [2] we explain our calculation scheme of the proton-nucleus elastic scattering amplitude for a Slater determinant wave function constructed from harmonic-oscillator single-particle orbits.

Let us start with the p -nucleus elastic-scattering amplitude already given by Eq. (1),

$$F(\mathbf{q}) = \frac{iK}{2\pi} \int d\mathbf{b} e^{i\mathbf{q}\cdot\mathbf{b}} \left(1 - e^{i\chi_N(\mathbf{b})} \right), \quad (\text{B1})$$

where \mathbf{b} is the impact parameter vector perpendicular to the beam (z) direction, \mathbf{K} the initial momentum of the relative motion, and \mathbf{q} the momentum transferred from the projectile to the target.

As we have shown in Eq. (2), $\chi_N(\mathbf{b})$ is the nuclear part of the optical phase-shift function given by

$$\begin{aligned}e^{i\chi_N(\mathbf{b})} &= \langle \Psi_0 | \prod_{i=1}^A \left[1 - \frac{1 + \tau_{3i}}{2} \Gamma_{pn}(\mathbf{b} - \mathbf{s}_i) \right. \\ &\quad \left. - \frac{1 - \tau_{3i}}{2} \Gamma_{pp}(\mathbf{b} - \mathbf{s}_i) \right] | \Psi_0 \rangle \\ &= \langle \Psi_0 | O(\mathbf{b} - \mathbf{s}) | \Psi_0 \rangle,\end{aligned}\quad (\text{B2})$$

where Ψ_0 is the intrinsic (translation-invariant) A -nucleon wave function of the nuclear ground state. The coordinate \mathbf{s}_i is the projection onto the xy -plane of the nucleon coordinate relative to the center-of-mass of the nucleus, *i.e.*, $\mathbf{s}_i = \mathbf{s}'_i - \mathbf{X}$, where \mathbf{s}'_i is the coordinate of a nucleon in the nucleus projected onto the xy -plane, and \mathbf{X} is the center-of-mass coordinate of the nucleus. τ_{3i} is 1 for neutron and -1 for proton. For later convenience, here we introduce an operator $O(\mathbf{b} - \mathbf{s})$.

The main idea is that, for the harmonic-oscillator Slater determinant wave function, the elastic scattering amplitude $F'(\mathbf{q})$ referring to the coordinate origin is factorized into a center-of-mass part and the intrinsic amplitude $F(\mathbf{q})$ [2], where $F'(\mathbf{q})$ is defined by

$$\begin{aligned}F'(\mathbf{q}) &= \frac{iK}{2\pi} \int d\mathbf{b} e^{i\mathbf{q}\cdot\mathbf{b}} \langle \Psi | \delta^{(3)}(\mathbf{X} - (1/A) \sum_j \mathbf{r}_j) \\ &\times (1 - O(\mathbf{b} - \mathbf{s}')) | \Psi \rangle,\end{aligned}\quad (\text{B3})$$

For the harmonic oscillator, $|\Psi\rangle$ is exactly factorized as $|\Psi\rangle = |\Psi_{cm}\rangle |\Psi_0\rangle$.

Then, the intrinsic amplitude which is free from the center-of-mass motion is easily calculated from $F'(\mathbf{q})$ as

$$F'(\mathbf{q}) = \langle \Psi_{cm} | e^{-i\mathbf{q}\cdot\mathbf{X}} | \Psi_{cm} \rangle F(\mathbf{q}), \quad (\text{B4})$$

where

$$\langle \Psi_{cm} | e^{-i\mathbf{q}\cdot\mathbf{X}} | \Psi_{cm} \rangle = \exp[-\nu^2 q^2 / 4A], \quad (\text{B5})$$

and ν is the size parameter of the harmonic-oscillator potential. The separability of the elastic scattering amplitude, Eq. (B3), is valid when the size parameter of the harmonic well for protons, ν_p , is equal to that for the neutrons, ν_n , which is the case for ^{16}O . On the other hand, when $\nu_p \neq \nu_n$, which is the case for $^{20,21,22}\text{O}$, we only assume this separability and adopt the following relation [3]:

$$\nu^2 = \frac{Z}{A} \nu_p^2 + \frac{N}{A} \nu_n^2. \quad (\text{B6})$$

Now, we focus on the calculation of the elastic scattering amplitude $F'(\mathbf{q})$ using the nucleon coordinates referring to the coordinate origin. Since we represent the ground-state wave function as a Slater determinant,

$$\Psi = (A!)^{-1/2} \det[\psi_m(r'_n)], \quad (\text{B7})$$

the antisymmetrization is only required for the bra, such as

$$\langle \Psi | = (A!)^{-1/2} \det[\delta_{mn} \psi_m^\dagger(r'_n)]. \quad (\text{B8})$$

As one can see from Eq. (B2), the operator $O(\mathbf{b} - \mathbf{s}')$ is factorizable into the operators that act on one particle subspaces, so that

$$\langle \Psi | O(\mathbf{b} - \mathbf{s}') | \Psi \rangle = \det[O_{nm}]_n \det[O_{nm}]_p, \quad (\text{B9})$$

where $\det[O_{nm}]_p$ is the $Z \times Z$ determinant for Z protons (in this work, $Z = 8$) and $\det[O_{nm}]_n$ is the $N \times N$ determinant for N neutrons. O_{nm} is the matrix element defined by

$$O_{nm} = \delta_{nm} - \int \psi_m^*(\mathbf{r}') \Gamma(\mathbf{b} + \mathbf{s}') \psi_n(\mathbf{r}') d\mathbf{r}'. \quad (\text{B10})$$

We have calculated the matrix element, O_{nm} , analyti-

cally and obtained the determinants [2]. Concerning the neutron part, $\det[O_{nm}]_n$, we take the average of the determinants of different configurations. For example, for ^{20}O , which has a 0^+ ground state, we have 12 neutrons, four of which are in the $0d_{5/2}$ state. Therefore, we have three different determinants that give a 0^+ ground state of ^{20}O .

-
- [1] R.J. Glauber, in *Lectures in Theoretical Physics* (Interscience, New York, 1959), Vol. 1, p.315.
- [2] R.H. Bassel and C. Wilkin, *Phys. Rev.* **174**, 1179 (1968).
- [3] W. Horiuchi, Y. Suzuki, B. Abu-Ibrahim, and A. Kohama, *Phys. Rev. C* **75**, 044607 (2007); Erratum: *ibid. C* **76**, 039903 (2007).
- [4] B. Abu-Ibrahim, W. Horiuchi, A. Kohama, and Y. Suzuki, *Phys. Rev. C* **77**, 034607 (2008).
- [5] A. Ozawa, T. Suzuki, and I. Tanihata, *Nucl. Phys.* **A 693**, 32 (2001).
- [6] A. Ozawa, O. Bochkarev, L. Chulkov, D. Cortina, H. Geissel *et al.*, *Nucl. Phys.* **A 691**, 599 (2001):
- [7] H. Masui, K. Kato, and K. Ikeda, *Phys. Rev. C* **73**, 034318 (2006).
- [8] G. A. Lalazissis, D. Vretenar, and P. Ring, *Phys. Rev. C* **63**, 034305 (2001).
- [9] Y. Kanada-Enfyo and Y. Akaishi, *Phys. Rev. C* **69**, 034306 (2004).
- [10] P. Saviankou, F. Grümmer, E. Epelbaum, and S. Krewald, *Phys. of Atomic Nucl.*, **69**, 119 (2006).
- [11] H. Nakada, *Nucl. Phys.* **A 764**, 117 (2006); Erratum: *ibid. A* **801**, 169 (2008).
- [12] J.K.Jewell, L.A.Riley, P.D.Cottle, K.W.Kemper, T.Glasmacher *et al.*, *Phys. Lett.* **B 454**, 181 (1999).
- [13] H. De Vries, *Atomic Data and Nuclear Data Tables*, **36**, 495 (1987).
- [14] R.F. Carlson, *Atomic Data and Nuclear Data Tables* **63**, 93 (1996).
- [15] A. Ingemarsson, *Nucl. Phys.* **A653**, 341 (1999).
- [16] Y. Suzuki, R.G. Lovas, K. Yabana, and K. Varga, *Structure and Reactions of Light Exotic Nuclei* (Taylor & Francis, London, 2003).
- [17] A. Kohama, K. Iida, and K. Oyamatsu, arXiv:0803.0187 [nucl-th].
- [18] Y. Ogawa, K. Yabana, and Y. Suzuki, *Nucl. Phys.* **A543**, 722 (1992).
- [19] A. Ozawa *et al.*, *Nucl. Phys.* **A709**, 60 (2002) [Erratum: *Nucl. Phys.* **A727**, 465 (2003)].
- [20] R. Kanungo, I. Tanihata, and A. Ozawa, *Phys. Lett.* **B 512**, 261 (2001).
- [21] B.A. Brown, *Prog. Part. Nucl. Phys.* **47**, 517 (2001).
- [22] R. Kanungo, M. Chiba, N. Iwasa, S. Nishimura, A. Ozawa *et al.*, *Phys. Rev. Lett.* **88**, 142502 (2002).
- [23] E. Sauvan, F. Carstoiu, N.A. Orr, J.S. Winfield, M. Freer *et al.*, *Phys. Rev. C* **69**, 044603 (2004).
- [24] D. Cortina-Gil, J. Fernandez-Vazquez, T. Aumann, T. Baumann, J. Benlliure *et al.*, *Phys. Rev. Lett.* **93**, 062501 (2004).
- [25] C. Nociforo, L.L. Jones, L.H. Khiem, P. Adrich, T. Aumann *et al.*, *Phys. Lett.* **B 605**, 79 (2005).
- [26] Z. Elekes, Zs. Dombrádi, N. Aoi, S. Bishop, Zs. Fülöp *et al.*, *Phys. Rev. Lett.* **98**, 102502 (2007).
- [27] A. Schiller, N. Frank, T. Baumann, S. Bazin, B.A. Brown *et al.*, *Phys. Rev. Lett.* **99**, 112501 (2007).
- [28] S. Terashima, private communication, and S. Terashima, H. Takeda, H. Otsu, K. Yoneda, T. Ichihara *et al.*, *RIKEN Accel. Prog. Rep.* **40**, 18 (2007).